HHS Public Access

Author manuscript

Biomaterials. Author manuscript; available in PMC 2022 August 01.

Published in final edited form as:

Biomaterials. 2021 August ; 275: 120775. doi:10.1016/j.biomaterials.2021.120775.

Delayed Neutrophil Recruitment Allows Nascent *Staphylococcus aureus* Biofilm Formation and Immune Evasion

Brian A. Pettygrove[#1,2], **Rachel M. Kratofil**[#3,4], **Maria Alhede**[5], **Peter Ø. Jensen**[5,6,7], **Michelle Newton**[3,4], **Klaus Qvortrup**[8], **Kyler B. Pallister**[2], **Thomas Bjarnsholt**[5,7], **Paul Kubes**[3,4], **Jovanka M. Voyich**[2], **Philip S. Stewart**[1,9]

[1]Center for Biofilm Engineering, Montana State University, Bozeman, MT, USA.

[2]Department of Microbiology and Immunology, Montana State University, Bozeman, MT, USA.

[3]Department of Physiology and Pharmacology, Cumming School of Medicine, University of Calgary, Calgary, AB, CA.

[4]Calvin, Phoebe and Joan Snyder Institute for Chronic Diseases, University of Calgary, Calgary, AB, CA.

[5]Costerton Biofilm Center, University of Copenhagen, Copenhagen, DK

[6]Institute for Inflammation Research, Center for Rheumatology and Spine Diseases, Copenhagen University Hospital, Rigshospitalet, Copenhagen, DK

[7]Department of Clinical Microbiology, Copenhagen University Hospital, Copenhagen, DK

[8]Department of Biomedical Sciences/CFIM, University of Copenhagen, Copenhagen, DK

[9]Department of Chemical and Biological Engineering, Montana State University, Bozeman, MT, USA.

[#] These authors contributed equally to this work.

Abstract

CrediT Author Statement

Brian A. Pettygrove: Conceptualization, Methodology, Formal Analysis, Investigation, Writing – Original Draft, Visualization
Rachel M. Kratofil: Conceptualization, Methodology, Formal Analysis, Investigation, Writing – Original Draft, Visualization
Maria Alhede: Investigation, Writing – Review & Editing
Peter Ø. Jensen: Investigation, Writing – Review & Editing
Michelle Newton: Investigation, Writing – Review & Editing
Klaus Qvortrup: Investigation, Writing – Review & Editing
Kyler B. Pallister: Validation, Resources, Writing – Review & Editing
Thomas Bjarnsholt: Conceptualization, Investigation, Writing – Review & Editing, Supervision, Funding Acquisition
Paul Kubes: Conceptualization, Methodology, Writing – Review & Editing, Supervision, Funding Acquisition
Jovanka M. Voyich: Conceptualization, Methodology, Writing – Review & Editing, Supervision, Funding Acquisition
Philip S. Stewart: Conceptualization, Methodology, Writing – Original Review & Editing, Supervision, Project Administration, Funding Acquisition

Declaration of interests

The authors declare that they have no known competing financial interests or personal relationships that could have appeared to influence the work reported in this paper.

Biofilms that form on implanted medical devices cause recalcitrant infections. The early events enabling contaminating bacteria to evade immune clearance, before a mature biofilm is established, are poorly understood. Live imaging *in vitro* demonstrated that *Staphylococcus aureus* sparsely inoculated on an abiotic surface can go undiscovered by human neutrophils, grow, and form aggregates. Small (~50 μm^2) aggregates of attached bacteria resisted killing by human neutrophils, resulting in neutrophil lysis and bacterial persistence. *In vivo*, neutrophil recruitment to a peritoneal implant was spatially heterogenous, with some bacterial aggregates remaining undiscovered by neutrophils after 24 hours. Intravital imaging in mouse skin revealed that attached *S. aureus* aggregates grew and remained undiscovered by neutrophils for up to three hours. These results suggest a model in which delayed recruitment of neutrophils to an abiotic implant presents a critical window in which bacteria establish a nascent biofilm and acquire tolerance to neutrophil killing.

Keywords

Staphylococcus aureus; biofilm; neutrophil; implant-associated infection; microscopy

Introduction

The bacterial or fungal biofilm state is often responsible for chronic, persistent infections on implanted surfaces and is an area of great concern to the medical community [1–4]. Biofilms that mature on implanted medical devices become recalcitrant to both antimicrobial therapies and host immune defenses [5–7]. Decades of research into novel biomaterial surfaces and antimicrobial coatings have yet to alleviate the issue. We suspect that an improved understanding of the innate immune response to an emergent biofilm is necessary to inform better strategies for preventing these serious infections.

Staphylococcus aureus readily forms biofilms on biotic and abiotic surfaces and has been a persistent threat to public health both in hospital-associated and more recently, community-associated infections [8, 9]. In addition to causing skin and soft tissue infections, sepsis, and necrotizing pneumonia, both methicillin-resistant and sensitive strains of *S. aureus* are common culprits in implant-associated infections, especially periprosthetic joint infections (PJI) and orthopedic implants [9–13]. Two-stage revision, one of the most used procedures to treat PJI, is expensive, prolonged (6 – 12 weeks), and only has a success rate between 65 to 90 percent [14, 15]. As is often the case in PJI, removal of an infected implant is frequently necessary to resolve biofilm infections [12, 14, 15]. In addition to causing serious harm to the patient, joint infections significantly increase economic costs, with studies finding total joint arthroplasty infection can triple or quadruple costs in Europe and the United States, respectively [16, 17].

In addition to forming biofilms, *S. aureus* expresses potent immunomodulatory virulence factors, making it an ideal organism to study host-pathogen interactions on a surface [18]. Mature *S. aureus* biofilms have been shown to utilize several mechanisms to modulate host immune responses such as inducing premature neutrophil extracellular trap (NET) formation [19], inhibiting complement [20], preventing phagocytosis [21, 22] and attenuating the anti-

bacterial activity of macrophages [23]. These and other studies have identified numerous strategies used by mature *S. aureus* biofilms to interfere with the normal host immune defenses. Nevertheless, it is unclear how, and at what stage in biofilm formation tolerance to host immune defenses manifests.

Previously, we have demonstrated that clearance of *S. aureus* aggregates attached to an abiotic surface *in vitro* depended on high densities of human neutrophils [24]. In addition, the aggregate size appears to play a role in the efficiency of phagocytosis [25]. Therefore, it is reasonable to hypothesize that clearance of a contaminated surface *in vivo* would require fast recruitment and high densities of neutrophils. Neutrophil recruitment *in vivo* is thought to occur within a few hours (2 – 4 h) after infection or injury [26, 27] and this timeframe may serve as a critical window for bacteria to establish biofilm aggregates. To our knowledge, this time scale of recruitment has not been investigated in the context of an implanted surface. In this present study, we hypothesized that delayed neutrophil recruitment to a *S. aureus*-contaminated implant site allows for nascent biofilm formation and tolerance to host defenses *in vivo*.

For successful clearance of contaminating bacteria to occur, we hypothesize that the following steps must occur: (i) Neutrophils must be recruited to the contaminated surface, via host- or pathogen-derived signals; (ii) Neutrophils must adhere to and patrol the surface in search of bacteria; (iii) Contaminating bacteria must be discovered by recruited neutrophils; and (iv) Neutrophils must phagocytose and successfully kill the discovered bacteria. We contend that these events must occur in a timely manner, before *S. aureus* biofilm aggregates develop tolerance to host defenses.

In this work, we investigated how small (~5–100 μm^2) *S. aureus* aggregates evade phagocytosis and killing by neutrophils by challenging adherent bacteria with human neutrophils *in vitro* during the early stages of biofilm formation. We additionally explored the dynamics of early neutrophil recruitment to a *S. aureus* contaminated surface using *in vivo* intravital imaging and neutrophil localization using a peritoneal implant model. Of note, we observed that human neutrophils readily clear lone cells or small groups of *S. aureus*. However, *S. aureus* rapidly becomes resilient through the formation of multicellular aggregates. *In vivo*, we observed that neutrophil recruitment is spatially and temporally heterogenous and can take several hours to occur, potentially providing sufficient time for contaminating microorganisms to mount mechanical and leukotoxic defenses prior to engagement by leukocytes.

Materials and Methods

Bacteria and neutrophil preparation

Staphylococcus aureus strain AH2547 (HG001 + pCM29, courtesy of Alex Horswill), a known biofilm-forming strain [36] and MW2-GFP (MW2 + pCM29) [37] with constitutive expression of a green fluorescent protein, was grown overnight in tryptic soy broth supplemented with 10 μg/ml chloramphenicol. Overnight cultures were centrifuged for 5 minutes at 4000 rpm, rinsed, resuspended in phosphate buffered saline (PBS), and serially diluted. Cells were attached to a 4-chambered glass bottom petri dish (Cellvis, CA, USA) to

facilitate live-cell imaging. To attach cells, varied concentrations of cells were added to the surface in PBS at a volume of 10 μL. After 30 minutes of incubation at 37°C, unattached bacteria were gently rinsed from the surface with PBS. Each chamber of the petri dish was filled with 1 ml of 10% fresh human serum in Hank's Balanced Salt Solution (HBSS) with Ca^{2+} and Mg^{2+} to simultaneously coat the surface with serum and opsonize bacteria and incubated at 37°C for 30 min. Human neutrophils were isolated from heparinized venous blood obtained from healthy donors following a standard IRB-approved protocol as described previously. All donors provided written consent to participate in the study. Neutrophils were isolated under endotoxin-free conditions (<25 pg ml^{-1}) and purity (<1% PBMC contamination) and viability (<2% propidium iodide positivity) of neutrophil preparations were assessed by flow cytometry as previously described [38, 39]. Neutrophils were kept on ice until stained with LysoBrite™ Red (AAT Bioquest, CA, USA) according to the manufacturer's instructions. Propidium iodide was added to the bulk medium just prior to neutrophil addition at a concentration of 5 μg/ml. To enumerate surviving bacteria, bacteria were removed from the surface using a sterile scraper and pipetting, vortexed in dilution tubes with PBS, and plated on tryptic soy agar in triplicate. Plates without detectable bacteria were counted as 0.5 colonies prior to log transformation.

Microscopy

A Leica SP5 inverted confocal scanning microscope was utilized for all *in vitro* imaging. GFP-tagged bacteria and neutrophils were excited with the 488 nm and 561 nm laser lines, respectively. A LiveCell (Pathology Devices, CA, USA) environmental chamber system was utilized to maintain 5% CO_2, 20% O_2, 50% humidity, and 37°C for sample incubation duri ng imaging. Image stacks with 1-μm z-slices were recorded sequentially at 1–2 min intervals over a 4-h time course using a 20X objective lens. At least two fields of view from each chamber of the dish were generally imaged per experiment. Each well was then imaged using a 7 × 7 stitched tile scan image with a 10x objective to quantify total amount of bacteria and count neutrophils remaining on the surface.

Image analysis

MetaMorph version 7.8.13 (Molecular Devices) image analysis software was used to measure the change in bacterial biomass by quantifying the threshold area of bacterial green fluorescence over the period of 4 h. Maximum growth rates were calculated by fitting an exponential curve to the data within log phase. Movies were prepared with Imaris version 8.0, 9.2, or 9.3 (Bitplane). To quantify neutrophil motion, the "Spots" module in Imaris was utilized to track 3D-objects over time, display their path, and analyze their motion. Neutrophils were automatically identified as "Spots" based on size and manually edited and confirmed when needed. Motion was tracked using the Brownian motion algorithm. To quantify the fraction of a field of view "patrolled" by a neutrophil over 4 hours, neutrophil tracks determined by the "Spots" module were set to be cylinders 10.87 μm in diameter. The image was then imported into MetaMorph, and the percentage of the field of view covered by a neutrophil track was determined by thresholding.

For the analysis of individual neutrophil-bacteria interactions, the "Spots" feature was used to identify neutrophils and propidium iodide staining events and the "Surfaces" feature was

used to dynamically track bacterial growth. From the 4 experiments, two fields of view for each condition were analyzed. 8 interactions per field of view were analyzed for control wells (8 fields of view × 8 interactions, n = 64) while all interactions that could reasonably be distinguished in the head start wells were analyzed (8 fields of view, n = 70 interactions). Measurements of the bacterial aggregate were recorded at the start and end of each interaction with a neutrophil, and propidium iodide staining or aggregate breakup events were cataloged. The percentage of aggregates inducing PI staining was calculated by dividing the number of aggregates that caused PI staining of at least one phagocytosing neutrophil by the total number of aggregates discovered by a neutrophil in each field of view.

Maximum growth rates of individual aggregates were calculated by fitting an exponential curve to volume measurements calculated using “Surfaces” in Imaris. Aggregates that were not detected for at least 88% of the frames were discarded. To determine the change in bacterial biomass over time from *in vivo* experiments, Imaris surface output files were analyzed in MATLAB and the total GFP volume (μm^3) was calculated for each frame. Percent change in biomass was calculated by comparing the last frame to the first frame for the final continuous field of view in each position. *In vivo* growth rates were calculated by fitting an exponential curve to the data collected in a continuous field of view that appeared to be out of lag phase and free of significant signal noise (such as due to animal movement).

Leukocyte counts from SEM images were produced by manually counting all visible cells that could be distinguished as distinct leukocytes and normalizing to the field of view area.

All images and videos from obtained from intravital microscopy were analyzed using Imaris version 9.5.1. GFP *S. aureus* clusters were quantified over time using the surface function and volume and neutrophil recruitment was tracked using the spot function. For quantification of neutrophil migration within the top 20 μm of collagen, spots were filtered for any spot entering the defined area of interest, top 20 μm of collagen, in the z-plane. Discovery frequency was quantified by applying a filter to the GFP bacteria surface “intensity mean” of tdTomato channel and thresholding was automatically applied by default settings.

Peritoneal implant model

The peritoneal implant model was performed as previously described with modifications [28, 29, 40]. Overnight cultures of *S. aureus* strain HG001 were grown in TSB for 20 h with shaking at 150 rpm and resuspended in 5 ml TSB before dilution. Sterile silicone tubes (i.d. 4 mm, o.d. 6 mm, length 4 mm) were incubated in a diluted overnight culture of *S. aureus* in 0.9% saline (OD_{600} = 0.1) for 1 hour at 100 rpm. Female C57bl/6JRj mice were purchased from Janvier and allowed two weeks to acclimate prior to surgery. Mice were anaesthetized with Hypnorm-midazolam (Hypnorm [0.315 mg fentanyl citrate/ml and 10 mg fluanisone/ml] and midazolam [5 mg/ml] and sterile water [1:1:2]) via subcutaneous injection in the groin area. 1 ml sterile PBS was injected into the mouse peritoneum 4h prior to implantation. Implants were inserted into the peritoneal cavity via a 1 cm groin incision. The mice were given bupivacaine and Temgesic for postoperative pain and euthanized by cervical dislocation at the end of the experiment. Several implants were removed and fixed

in 2% glutaraldehyde for analysis by scanning electron microscopy while the remaining implants were put in 2 ml 0.9% NaCl and kept on ice until further processing. To quantify colony forming units on implants pre-insertion, representative silicone tubes were sonicated in 0.9% saline and dilutions were plated on tryptic soy agar. To determine the number of neutrophils recruited to the peritoneum, a lavage was performed by injecting 5 ml of PBS into the peritoneal cavity and gently massaging the abdomen before withdrawing the peritoneal fluid (PF) [41]. PF was stored on ice until preparing the samples for determination of recovered neutrophils by flow cytometry. To enumerate the neutrophils in the PF a 100 μl sample was added to a TruCount Tube (340334, Becton Dickinson). Ten μl of Anti-Ly-6C-FITC, mouse (130-102-295, Miltenyi Biotec), Anti-Ly-6G-APC, mouse (130-102-342, Miltenyi Biotec), and CD45-PerCP, mouse (130-102-469, Miltenyi Biotec) were added and the samples were incubated on ice for 30 min in the dark before fixation by addition of 1 ml of 10% (v/v) FACS lysing solution (349202, Becton Dickinson). Stained and fixed samples were analyzed by flow cytometry using a FACSCanto II (Becton Dickinson). Light scatter and fluorescence parameters for >10 000 events were recorded after gating on forward light scatter and fluorescence for CD45 staining to exclude debris, cell aggregates and bacteria. The instrument was calibrated with CSTbeads (Becton Dickinson, Franklin Lakes, NJ, USA). All experiments were authorized by the National Animal Ethics Committee, Denmark, Permit number 2018-15-0201-01500.

Scanning electron microscopy

Specimens were fixed in 2% glutaraldehyde in 0.05 M sodium phosphate buffer, pH 7.4. Following 3 rinses in 0.15 M sodium phosphate buffer (pH 7.4) specimens were post fixed in 1% OsO4 in 0.12 M sodium cacodylate buffer (pH 7.4) for 2 h. Following a rinse in distilled water, the specimens were dehydrated in 100% ethanol according to standard procedures and critical point dried (Balzers CPD 030) with CO_2. The specimens were subsequently mounted on stubs using double adhesive carbon tape (Ted Pella) as an adhesive and sputter coated with 6 nm gold (Leica ACE 200). Specimens were examined with a Quanta 3D SEM (FEI, Eindhoven, The Netherlands) operated at an accelerating voltage of 2 kV.

Intravital imaging in a murine skin flap model

Animal experiments were performed with male adult 7–8-wk-old mice and all experimental animal protocols were approved by the University of Calgary Animal Care Committee and followed guidelines established by the Canadian Council for Animal Care (protocol number AC19-0138). All mice were housed under specific pathogen-free conditions and received sterilized rodent chow and water *ad libitum*. Catchup$^{IVM\text{-}red}$ mice in which neutrophils are tagged with a tdTomato red fluorescent protein were anesthetized and kept at body temperature using a heating pad [31]. A jugular catheter was inserted to maintain anesthesia and deliver systemic treatments. The dorsal flank skin was exteriorized on the right flank as previously described [26]. The tissue was covered with a cover slip that had been seeded with GFP-tagged *S. aureus* at surface densities similar to those used in *in vitro* experiments (10^3–10^4 CFU/cm^2, pregrown in RPMI medium, rinsed with HBSS). Superfusion buffer (HBSS without calcium, magnesium, or phenol red, ThermoFisher) was then perfused across the exteriorized skin tissue to keep the skin moist at a flow rate set to 0.17 ml/min.

Mice were imaged for up to 180 min after being anesthetized using a Leica SP8 upright multiphoton microscope. Laser excitation at 940 nm was used to excite tdTomato and GFP with external detectors (HyD-RLD2 BP 585/40 for tdTomato, HyD-RLD3 BP 525/50 for GFP) and second harmonic generation (external detector HyD-RLD4 BP 450/70) to visualize skin collagen. Laser power, detector settings and acquisition settings were maintained throughout each experiment. Blood vasculature was labeled intravascularly using Qtracker™ 655 Vascular Labels (ThermoFisher) with excitation/emission at 405–615/655 nm (external detector HyD-RLD1 BP 675/50).

A 3D tile scan (4×4 fields of view; each field of view 350 × 350 × 100 μm^3) was first collected to get an overview of the GFP *S. aureus* aggregates on the coverslip. From there, 3 fields of view (350 × 350 × 80 μm^3) were selected within the 3D tile scan to select the video positions. Images were collected every 45 s for up to 180 min.

Statistical treatment of data

Data were analyzed using GraphPad Prism version 8.4.2. Normality was assessed by the D'Agostino-Pearson or Shapiro-Wilk test. Normal data was tested with an unpaired student's t test, one-way ANOVA with Tukey's post hoc test, two-way ANOVA with Bonferroni's or Tukey's multiple comparisons test or Brown-Forsythe ANOVA with Dunnet's T3 multiple comparisons test as appropriate. Otherwise, the Kruskal-Wallis test or Mann-Whitney test was applied. The test applied is described in each figure legend.

Data Availability

The raw and processed data required to reproduce these findings are available to download from https://datadryad.org/stash/share/WHrJoeXSaqg3jdFH9pOPwUlablkGwl2RVvFePLu3fc4.

Results

High surface densities of neutrophils are required for effective clearance of *S. aureus*

We utilized an *in vitro* confocal microscopy approach to observe interactions between adherent *S. aureus* and human neutrophils (polymorphonuclear leukocytes, PMNs). Green fluorescent protein (GFP) expressing *S. aureus* AH2547 was sparsely seeded on a glass surface, challenged with fluorescently labeled neutrophils, and continuously imaged for 4 h. In the absence of neutrophils, bacteria grew and formed dense aggregates on the surface with a collective specific growth rate of 0.80 ± 0.16 h^{-1}. Interestingly, the growth rate of individual *S. aureus* aggregates was quite variable, ranging from −0.2 to 1.6 h^{-1} (Figure S1A). Clearance of bacteria was highly dependent on the density of neutrophils on the surface, with effective killing occurring under higher neutrophil conditions (Figures 1A and 1B). Low neutrophil conditions resulted in killing of some attached bacterial aggregates, but survival and prolific growth of the many undiscovered aggregates. Conversely, sufficiently high neutrophil concentrations allowed rapid discovery and elimination of adherent bacteria before aggregates were able to grow significantly (Figures 1A and 1B). Neutrophil surface densities greater than 10,000 neutrophils/cm^2 often enabled effective clearance of bacteria, resulting in 1.5 – 2 log reductions in bacterial burden compared to control wells without

neutrophils (Figure 1C). Clearance of the bacteria correlated well with the ability of neutrophils to “patrol” large surface areas (Figure 1D). Net bacterial growth as measured by GFP area within a given field of view (FOV) was halted when approximately 50% of the surface was patrolled and reductions in bacterial burden greater than one log were consistently observed at approximately 80% coverage of the surface by neutrophil tracks (Figure 1D). When densities of both neutrophils and bacteria were low, the outcome was stochastic and the result often depended on timely discovery of the bacteria, which we have previously described in a mathematical model [24]. Thus, we have observed that a high surface density of neutrophils is required to effectively discover and eliminate *S. aureus* sparsely adherent to an abiotic surface.

Neutrophil recruitment to a peritoneal implant is heterogeneous

To observe spatial patterns of immune cell recruitment to a contaminated biomaterial *in vivo*, we utilized a previously described murine peritoneal implant model [28, 29]. A silicone tube was homogeneously coated with a low density of *S. aureus* and inserted into the mouse peritoneum via groin incision. Mice were euthanized 24 h post implantation and the implants were removed for analysis. We estimated the initial bacterial burden on the implant surface to be approximately $4.1 \pm 1.7 \times 10^5$ CFUs/implant via plate count and $1.2 \pm 0.51 \times 10^6$ cells/cm^2 based on counts from scanning electron microscopy (SEM) micrographs (n = 9 FOVs from 2 implants) (Figure 2A). After 24 h in the peritoneum, the mean log reduction of viable bacterial counts recovered from implants (referenced to the pre-insertion count) was 1.98 ± 0.73 (n = 11). Flow cytometry of immune cells collected by peritoneal lavage showed that neutrophils were highly prevalent in the mouse peritoneum at 24 hpi, constituting 53 ± 6.8 % of host cells (n = 8 mice), whereas the background levels of neutrophils in animals that did not receive an implant was 0.7 ± 0.8 % (n = 8). The concentration of neutrophils in peritoneal lavage fluid was $4.3 \pm 3.3 \times 10^3$ cells/ml in animals that did not receive an implant and rose to $4.1 \pm 0.9 \times 10^5$ cells/ml in animals harboring inoculated implants for 24 h. Interestingly, although the distribution of *S. aureus* appeared uniform across the implant surface prior to insertion, recruitment of immune cells to the implant was spatially heterogeneous. By SEM, we observed the formation of distinct patches of host material on the implant surface (Figure 2B). Examination of these patches at higher magnification revealed aggregations of leukocytes (Figure 2C). We estimated the local surface density of these leukocyte patches to be $6.2 \pm 5.6 \times 10^5$ leukocytes/cm^2 based on counts of observable cells in areas where leukocytes were present (n = 10 FOVs from 2 implants) (Figure 2F). Several FOVs were devoid of leukocytes (Figure 2F). Magnification of areas lacking these leukocyte patches revealed that *S. aureus* aggregates remained on the surface with little to no interaction with recruited immune cells (Figure 2D). Additionally, while the SEM images of implants pre-insertion revealed mostly single or paired groupings of *S. aureus* cells (Figure 2A), the areas without recruited immune cells on explanted surfaces contained clusters of *S. aureus* with larger numbers of cells, suggesting growth (Figure 2E). These observations support the hypothesis that some bacteria on a contaminated surface may escape detection due to heterogeneous recruitment of immune cells, providing these cells an opportunity to develop into more resilient aggregates.

S. aureus aggregates resist clearance by neutrophils *in vitro*

We have observed previously that *S. aureus* aggregates discovered by neutrophils later in an *in vitro* experiment tended to be more tolerant to neutrophil clearance [24]. Therefore, we sought to further investigate and quantify the effect of aggregate size and timing of discovery on *S. aureus* survival of neutrophil challenge. *S. aureus* was sparsely seeded on glass and then allowed to form aggregates for 4 h prior to the addition of neutrophils. In control wells without neutrophils, preformed *S. aureus* aggregates grew into larger aggregates on the surface after 4 h of imaging (Fig. 3Ai–ii). Clusters of *S. aureus* that were given a 4 h head start prior to the addition of neutrophils resisted clearance, resulting in large aggregates remaining on the surface at the end of the experiment (Figure 3Aiii–iv). However, CFU-matched single-cell *S. aureus* were readily cleared by the neutrophils within 4 h (Figure 3Avii–viii). We quantified the log CFU of *S. aureus*/cm^2 in the presence and absence of neutrophils for both head start (4 h) and no head start (single-cell *S. aureus*) and found that in the presence of neutrophils, there was a significant reduction of *S. aureus* recovered from the surface post-imaging (Figure 3B). Furthermore, neutrophils were significantly more effective at clearing single-cell *S. aureus* compared to preformed aggregates (Figure 3C). This suggests that surface attachment alone is not an inherent barrier to neutrophil clearance, but within a short period of time *S. aureus* aggregates can develop tolerance to neutrophils.

We observed that some aggregates failed to decrease in size after co-localization with a neutrophil and that some neutrophils disappeared during this interaction. These observations led us to investigate whether larger *S. aureus* aggregates were lysing neutrophils. We added propidium iodide (PI), a membrane impermeable dye, to our assay to investigate whether neutrophil membrane integrity was compromised upon interaction with large *S. aureus* aggregates. Neutrophils interacting with larger aggregates often stained extensively with PI, suggesting these aggregates were able to damage neutrophil membrane integrity (Video S1). Neutrophils became PI positive at a much higher frequency when *S. aureus* aggregates were given a head start prior to the addition of neutrophils (Figures 4A–C). Under the head start condition, 86 ± 19% of aggregates in a given FOV induced PI staining of at least one neutrophil while we did not observe any single cells of *S. aureus* causing PI staining of neutrophils in this assay (Figure 4C, Video S1). We analyzed the outcome for each bacterial aggregate present in a field of view and found that aggregates greater than roughly 50 μm^2 caused frequent neutrophil lysis and aggregates greater than 75 μm^2 caused neutrophil lysis in all of the interactions observed in these experiments (Figure 4D). Larger aggregates tended to persist, as aggregates with initial area greater than 75 μm^2 at the time of interaction with a neutrophil often failed to decrease or even grew in size from the time of discovery (Figure 4E). We also observed on occasion that large aggregates could be broken up or fractured into smaller pieces by multiple neutrophils and that these smaller pieces were more readily cleared (Video S2). These events did not seem to depend solely on the size of the aggregate (Figure S2A). Rather, aggregates appeared to fracture when a high number of neutrophils attempted to phagocytose a portion of the aggregate over the course of the experiment (Figure S2B). Non-fractured aggregates tended to grow slightly over the 4 h observation period following discovery by the first neutrophil, however when fracture occurred, there was a slight decrease in the total volume of all fractured pieces (Figure S2C).

This suggests a better outcome when neutrophils are successfully able to fragment a portion of the bacterial cluster compared to when the clusters remain intact.

Minimal neutrophil recruitment to a *S. aureus*-contaminated coverslip *in vivo*

We adapted a murine skin intravital microscopy model [26, 30] to visualize *in vivo* neutrophil behavior on a coverslip inoculated with bacteria in real time using resonant-scanning multiphoton intravital microscopy. This design paralleled the *in vitro* experiments described above. Approximately 10^4 CFUs of *S. aureus* AH2547 GFP were seeded onto a glass coverslip and allowed to grow for 4 h to form aggregates (head start) and the contaminated coverslip was interfaced with the dermis. With the multiphoton system, dermal collagen was visualized via second harmonic generation (SHG), neutrophils were fluorescently labeled with tdTomato in the Catchup$^{IVM\text{-}red}$ reporter mouse [31] and *S. aureus* was visualized with GFP. Previously, it has been shown that neutrophils are robustly recruited to a localized *S. aureus* infection in the skin within 2 h [26], so we asked whether neutrophils were recruited in a similar timeline to *S. aureus* aggregates on a coverslip. Over the course of 180 min, there was minimal neutrophil recruitment to the *S. aureus* coverslip surface (Figures 5A–C, Video S3). In many FOVs, we observed zero or one neutrophil and the one neutrophil was often deeper in the collagen away from the *S. aureus* aggregates (Figure 5A). In the rare occurrence where we saw neutrophil recruitment (Figure 5B), we quantified how many neutrophils migrated towards the *S. aureus* aggregates within the top 20 μm of collagen (Figures 5D–E). We recorded three FOVs per mouse (from n = 4 independent experiments) and observed around 10 neutrophils migrate into the top 20 μm of collagen in only two of the twelve FOVs (Figure 5D), suggesting very few neutrophils are recruited to the *S. aureus*-contaminated coverslip *in vivo* during these early time points. Of those neutrophils that were able to migrate towards the coverslip surface, we further quantified how many associated with *S. aureus* aggregates (Figure 5F) and found again that few neutrophils were interacting with *S. aureus* (Figures 5F and 5G, Video S4). To confirm these results, we repeated the experiment using a clinically relevant methicillin-resistant *S. aureus* strain MW2 and again observed minimal neutrophil recruitment (Figure S3). Using single-cell *S. aureus* attached to the coverslip for 30 min (no head start), we observed no neutrophil recruitment to the coverslip over 180 min (Figure 5H). In many of the videos we occasionally observed one or two neutrophils, but this was transient as the neutrophils seemed to be passing by in deeper skin capillaries (data not shown). Importantly, there was no neutrophil recruitment to a sterile coverslip (Figure 5I). At the end of the 180 min of imaging, a fluorescent vascular dye was injected to visualize dermal blood vessels and capillaries within the dermal collagen (Figure 5J). This larger stitched image highlights that there was no neutrophil recruitment to a sterile coverslip, though we were able to detect one or two neutrophils within capillaries (Figure 5Ki–ii) and within larger dermal vessels (Figure 5Kiii).

Altogether, these data show that very few neutrophils are recruited to a *S. aureus* contaminated coverslip interfaced with the dermis over the course of 180 min *in vivo*. On the rare occasion where neutrophils migrated to the coverslip surface, they can interact with *S. aureus* aggregates, but the earliest this occurred was about 1–2 h after placing the coverslip

onto the skin. In most FOVs, neutrophil recruitment was not observed over the imaging window of 180 min.

S. aureus aggregates grow on the coverslip *in vivo*

To understand the dynamics of bacterial growth *in vivo*, we measured the increase in surface volume of *S. aureus* aggregates over the course of imaging. It was clear that the bacterial aggregates became larger from the time the coverslip was added to the skin (Figure 6A) to the end of imaging at 180 min (Figure 6B). *S. aureus* aggregates were closely associated with the collagen surface (Figure 6C) suggesting they are in physical contact with the host dermal tissue. *In vitro*, *S. aureus* required supplementation of HBSS with serum to grow, demonstrating that host factors were required to support bacterial growth and that the superfusion buffer (HBSS) alone would not explain the observed growth (Fig. S1B and S1C). We measured the growth rate of *S. aureus* over the three hours of imaging and found the average growth rate to be $0.46 \pm 0.45\ h^{-1}$ (median $0.25\ h^{-1}$) for strain AH2547, however significant heterogeneity was observed between FOVs (Figures 6D and 6E). Similar results were obtained with strain MW2 (Figures 6E, S3C). These data demonstrate that once the coverslip was placed in close contact with host tissue, bacteria started to grow and construct aggregate before neutrophils arrived.

Recruited neutrophils discover some aggregates *in vivo*

Next, we asked whether neutrophils pre-recruited to the skin with the chemokine macrophage inflammatory protein 2 (MIP-2) would affect bacterial aggregate discovery and clearance. Mice were treated with MIP-2 4 h before the start of imaging (Figure 7A). In contrast to experiments without MIP-2 treatment (Figure 5A and 5B), many neutrophils were present in the dermis at the outset (Figure 7B and 7C). Over the course of imaging, we did not see a significant increase in the number neutrophils indicating that no additional neutrophils were recruited into the dermis during this time (Figure 7B, S4A and S4B). Within an individual animal, neutrophil recruitment to the coverslip was also heterogeneous where some fields of view had more neutrophils than other FOVs from the same mouse (Figures S4C and S4D, Video S5). Although we did see neutrophils enter the field of view during the 180 min window (Figure S4C and S4D), this was not due to an increase in total neutrophil recruitment (Figure 7B, S4A and S4B) but a change in neutrophil localization (Figure 7C). At 10 min many of the neutrophils were 50–100 μm away from the *S. aureus* aggregates but by 180 min, the neutrophils migrated towards the coverslip and were much closer to the aggregates (Figure 7C). Indeed, we observed a significant change in neutrophil localization as neutrophils migrated 50–100 μm towards the bacterial aggregates in the z-plane, which suggests that the existing neutrophils pre-recruited by MIP-2 addition were able to migrate towards *S. aureus* (Figures 7C and 7D). After a 30 min single-cell attachment, many neutrophils chemotaxed towards the *S. aureus* single cells and migrated very close to the coverslip interface with a mean distance of 26 μm away from the bacterial aggregates (Figure 7D). We next compared this to a head start experiment where we allowed *S. aureus* aggregates to grow for 4 h to the coverslip. Although neutrophils did migrate towards these larger aggregates, there was strikingly a significant decrease in neutrophil localization and these neutrophils were much further away from the aggregates, with a mean distance of 42 μm away (Figure 7D). The frequency of aggregate discovery by neutrophils

was calculated using Imaris by applying a filter to the aggregate surface (Figure 7E, Video S6). When bacteria were only attached for 30 min, there was a significant increase in aggregate discovery between 10 min and 180 min (Figures 7F and 7G). At the 180 min time point, neutrophils more frequently discovered bacteria in the 30 minute attachment condition (45–75% discovery) compared to a 4 h biofilm (25–35% discovery) (Figures 7F, 7G, and S4E). Mice that were not treated with MIP-2 had negligible bacteria discovery (under 10% discovery) at the 180 min time point (Figures 7F, 7G and S4E). To identify any relationship between bacterial load and number of neutrophils recruited, we analyzed the trends of total bacterial surface volume at the 180 min time point against total number of neutrophils (Figure S4F). Interestingly, without MIP-2 pre-treatment we did not see a positive correlation between the number of neutrophils and the bacterial surface volume, suggesting that at these bacterial burdens and time points, increased bacterial biomass does not directly lead to increased neutrophil recruitment (Figure S4F).

Overall, pre-recruitment of neutrophils to the skin with MIP-2 led to a marked reduction in *S. aureus* aggregate volume over the course of the experiment when *S. aureus* was given a head start to form aggregates (Figure 7H). *S. aureus* only given 30 min to form aggregates saw a slight but not statistically significant reduction in volume after MIP-2 treatment (Figure 7H). This demonstrates that neutrophils must be present in high densities in order to have an effective response to remove the contaminating bacteria. Due to the limited imaging window of 180 min, we never observed full clearance of bacteria from the coverslip even with pre-recruitment of neutrophils, and some bacterial aggregates were left undiscovered for the entire 180 min of imaging (Figure 7G).

Discussion

S. aureus is a major pathogen of implant-associated infections and serious complications can arise if the device is not surgically removed. Presently, it is unclear how small amounts of bacteria evade the host immune system and establish an infection. These early events in the interaction between host and pathogen are currently under-studied and we therefore investigated initial interactions between neutrophils and nascent *Staphylococcus aureus* biofilms *in vitro* and *in vivo*.

We hypothesized that successful clearance of contaminating bacteria from an implant surface requires that neutrophils are recruited to the surface, adhere to and patrol the surface, discover contaminating bacteria, and successfully phagocytose and kill the bacteria. We confirmed that neutrophils are able to kill surface attached *S. aureus in vitro* if a sufficient number of neutrophils are present on the surface and if *S. aureus* did not have time to form nascent biofilm aggregates. Deficiencies in neutrophil recruitment could permit biofilm formation in two ways: 1) Delayed recruitment could lead to the formation of neutrophil-tolerant biofilm aggregates prior to the appearance of a robust innate immune response, 2) An insufficient number of neutrophils “patrolling” an implanted surface could result in some of the attached *S. aureus* remaining undiscovered, again allowing aggregate formation. While we may expect *in vivo* to see directed recruitment of neutrophils to contaminating organisms due to chemotactic gradients produced by local cells that may initially discover contaminating microorganisms (macrophages, epithelial cells, etc.), we clearly observed *in*

vivo that neutrophil recruitment can be highly heterogeneous. Thus, a high recruitment of neutrophils to an implanted surface is likely still important to enable full surface coverage and ensure that any contaminating microorganisms are destroyed promptly. Alternatively, during infection bacterial aggregates often exist in the peri-implant space and may not require direct neutrophil attachment to the surface for discovery. Robust recruitment to the peri-implant space to effectively discover these aggregates likely is still essential for clearance in this scenario.

We observed that *S. aureus* aggregates begin to demonstrate tolerance and the ability to lyse neutrophils at a relatively small aggregate size of approximately 50 μm^2. Accordingly, it is plausible that *S. aureus* requires only a small amount of time, perhaps on the order of hours, prior to the arrival of host innate immune defenses in order to be able to mount a defense and tolerate neutrophil challenge. *S. aureus* aggregates appear to resist clearance by neutrophils both by the physical protection afforded by forming an aggregate and elaboration of virulence factors. Aggregates broken up by several neutrophils appeared to be slightly more susceptible to neutrophil killing, highlighting a benefit for the microorganisms of developing a structurally durable aggregate. After four hours of aggregate formation, *S. aureus* caused significant cytotoxic damage to interacting neutrophils *in vitro*, likely due to the production of pore-forming toxins such as γ-hemolysin or Panton-Valentine leukocidin, resulting in persistence of the bacteria [18, 19]. These behaviors are strikingly similar to examples of classical biofilm behavior that facilitates immune evasion [19, 22, 32]. However, here we have shown that tolerance to neutrophil clearance is occurring at a very early stage in biofilm development while previous work has primarily investigated immune cell interactions with mature *in vitro* biofilms. While these aggregates are quite small compared to a typical *in vitro* biofilm, aggregates of similar sizes have been reported in several types of human biofilm infections, such as implant associated infections [33]. These results suggest that contaminating *S. aureus* may be able to quickly establish a biofilm aggregate that can become relatively protected from early host immune defenses.

To investigate the dynamics of neutrophil recruitment *in vivo*, we utilized a peritoneal implant model and a dermal intravital imaging model to characterize and quantify leukocyte recruitment to contaminated surfaces. At 24 h after peritoneal implantation, we observed highly heterogenous recruitment of immune cells to a *S. aureus* contaminated silicone implant. While immune cells were strongly recruited to certain areas of the implant, SEM of seemingly bare areas only a few millimeters away revealed persistence of *S. aureus* cells. This observation suggests that discovery of bacteria on an implant surface could take longer than 24 h in some models, allowing a window for bacteria to grow and form more resilient aggregates. This mirrors our measurements *in vitro* (Figure 1D). We hypothesize that these leukocyte patches observed could develop in part due to the expression of chemotactic factors following neutrophil discovery and phagocytosis of bacteria or abiotic debris. This phenomenon has been described in other contexts as neutrophil swarming and is driven by LTB4, a molecule known to be produced by neutrophils [34]. LTB4-dependent neutrophil swarming was originally described during sterile injury, but recently neutrophil swarming was also observed during a *S. aureus* infection in the lymph node, indicating that neutrophils are capable of swarming in the presence of bacterial infection [35]. Indeed, we observed both *in vitro* and *in vivo* that on occasion once neutrophils encountered a *S. aureus* aggregate

a neutrophil swarm formed (data not shown). The role of LTB4 in the control and clearance of *S. aureus* aggregates from a contaminated biomaterial is a mechanism we would like to pursue in future studies.

This study also used intravital microscopy to track the progression of *S. aureus* aggregate growth and neutrophil recruitment to the coverslip *in vivo*. First, we have demonstrated that once a contaminated coverslip is placed onto host tissue, bacteria are able to grow well before neutrophils can be recruited from the bloodstream. Robust neutrophil recruitment was not observed over 180 min of imaging, suggesting that a longer imaging window might be necessary to capture the onset of neutrophil recruitment in most cases. Although a previous *S. aureus* gel bead model resulted in neutrophil recruitment within 2 h [26], this disparity may have been due to a difference in dosage of bacteria (10^6 CFU/bead vs. 10^4 CFU/coverslip). It seems reasonable to assume that even the bacterial density utilized in our study would exceed the number of contaminating organisms present on an implant surface following surgery, suggesting delayed recruitment of neutrophils is plausible in human patients. Furthermore, differences in models (*S. aureus* bead vs. contaminated coverslip) could give rise to differences in neutrophil recruitment *in vivo*. We have also calculated the growth rate of *S. aureus* attached to a foreign object *in vivo*, which adds to the limited knowledge of *in vivo* bacterial growth rates reported. Since bacteria were able to grow significantly over the first 180 min, this indicates that early events are critical for bacteria to establish a protective niche.

We chose to use the chemokine MIP-2 as it is a potent chemoattractant to recruit neutrophils to sites of inflammation [27]. By pre-recruiting neutrophils, we were able to see aggregate discovery by neutrophils and a marked decrease in bacterial aggregate volume at the end of imaging, suggesting that neutrophils have the ability to clear contaminated surfaces *in vivo* if they reach the infected site quickly. However, future modification of the model will be necessary to follow up on this result, as we were unable to image for longer than three hours. It was also interesting that more neutrophils discovered aggregates that were only grown for 30 min compared to 4 h to form a biofilm, which highlights the importance of early bacterial discovery on contaminated implants before bacteria have the opportunity to form a biofilm.

Conclusion

In this work, we investigated the interactions between nascent *S. aureus* biofilms and human neutrophils *in vitro* and the recruitment dynamics of neutrophils *in vivo*. We observed a brief window of time where *S. aureus* aggregates are readily phagocytosed and killed by neutrophils if discovered, but these aggregates become more resilient once they exceed approximately 50 μm^2. Leukocyte recruitment to a peritoneal implant was heterogeneous after 24 h and we observed many undiscovered bacteria remaining on the surface, suggesting that discovery of contaminating microbes can take up at least 24 h. We also observed *in vivo* with intravital microscopy that minimal numbers of neutrophils were recruited to a contaminated coverslip placed onto a dermal skin flap within 3 h. Even though pre-recruitment of neutrophils with MIP-2 resulted in a decrease in bacterial aggregate volume, some aggregates remained undiscovered by neutrophils, suggesting robust recruitment is required for sterilization.

Future studies should further investigate the time scales and distribution of neutrophil recruitment times to a contaminated surface *in vivo* and the potential roles of other immune cell types during the early stages of infection. Identification of mechanisms used by *S. aureus* to evade neutrophils through toxin production and aggregation could help to better inform pathogenesis and suggest therapeutic targets. Finally, our results raise the intriguing proposition of artificially "boosting" neutrophil recruitment near an implanted surface as a prophylactic measure and we aim to explore the viability of this treatment in a variety of clinically relevant models.

Supplementary Material

Refer to Web version on PubMed Central for supplementary material.

References

[1]. Costerton JW, Stewart PS, Greenberg EP. 1999. Bacterial Biofilms: A Common Cause of Persistent Infections. Science 284:1318–1322. [PubMed: 10334980]

[2]. Gbejuade HO, Lovering AM, Webb JC. 2015. The role of microbial biofilms in prosthetic joint infections. Acta Orthop 86:147–158. [PubMed: 25238433]

[3]. Jacqueline C, Caillon J. 2014. Impact of bacterial biofilm on the treatment of prosthetic joint infections. J Antimicrob Chemother 69:i37–i40. [PubMed: 25135088]

[4]. Parsek MR, Singh PK. 2003. Bacterial Biofilms: An Emerging Link to Disease Pathogenesis. Annu Rev Microbiol 57:677–701. [PubMed: 14527295]

[5]. Jesaitis AJ, Franklin MJ, Berglund D, Sasaki M, Lord CI, Bleazard JB, Duffy JE, Beyenal H, Lewandowski Z. 2003. Compromised Host Defense on *Pseudomonas aeruginosa* Biofilms: Characterization of Neutrophil and Biofilm Interactions. J Immunol 171:4329–4339. [PubMed: 14530358]

[6]. Stewart PS. 2015. Antimicrobial Tolerance in Biofilms. Microbiol Spectr 3:10.1128/microbiolspec.MB-0010–2014.

[7]. Stewart PS, William Costerton J. 2001. Antibiotic resistance of bacteria in biofilms. The Lancet 358:135–138.

[8]. Dantes R, Mu Y, Belflower R, Aragon D, Dumyati G, Harrison LH, Lessa FC, Lynfield R, Nadle J, Petit S, Ray SM, Schaffner W, Townes J, Fridkin S. 2013. National Burden of Invasive Methicillin-Resistant *Staphylococcus aureus* Infections, United States, 2011. JAMA Intern Med 173:1970–1978. [PubMed: 24043270]

[9]. Kobayashi SD, DeLeo FR. 2009. An update on community-associated MRSA virulence. Curr Opin Pharmacol 9:545–551. [PubMed: 19726228]

[10]. Arciola CR, Campoccia D, Montanaro L. 2018. Implant infections: adhesion, biofilm formation and immune evasion. Nat Rev Microbiol 16:397–409. [PubMed: 29720707]

[11]. Kourbatova EV, Halvosa JS, King MD, Ray SM, White N, Blumberg HM. 2005. Emergence of community-associated methicillin-resistant *Staphylococcus aureus* USA 300 clone as a cause of health care-associated infections among patients with prosthetic joint infections. Am J Infect Control 33:385–391. [PubMed: 16153484]

[12]. Pulido L, Ghanem E, Joshi A, Purtill JJ, Parvizi J. 2008. Periprosthetic Joint Infection: The Incidence, Timing, and Predisposing Factors. Clin Orthop 466:1710–1715. [PubMed: 18421542]

[13]. Trampuz A, Piper KE, Jacobson MJ, Hanssen AD, Unni KK, Osmon DR, Mandrekar JN, Cockerill FR, Steckelberg JM, Greenleaf JF, Patel R. 2007. Sonication of Removed Hip and Knee Prostheses for Diagnosis of Infection. N Engl J Med 357:654–663. [PubMed: 17699815]

[14]. Kurtz SM, Lau E, Watson H, Schmier JK, Parvizi J. 2012. Economic Burden of Periprosthetic Joint Infection in the United States. J Arthroplasty 27:61–65.e1. [PubMed: 22554729]

[15]. Senthi S, Munro JT, Pitto RP. 2011. Infection in total hip replacement: meta-analysis. Int Orthop 35:253–260. [PubMed: 21085957]

[16]. Kapadia BH, McElroy MJ, Issa K, Johnson AJ, Bozic KJ, Mont MA. 2014. The Economic Impact of Periprosthetic Infections Following Total Knee Arthroplasty at a Specialized Tertiary-Care Center. J Arthroplasty 29:929–932. [PubMed: 24140271]

[17]. Puhto T, Puhto A-P, Vielma M, Syrjälä H. 2019. Infection triples the cost of a primary joint arthroplasty. Infect Dis 51:348–355.

[18]. Guerra FE, Borgogna TR, Patel DM, Sward EW, Voyich JM. 2017. Epic Immune Battles of History: Neutrophils vs. *Staphylococcus aureus*. Front Cell Infect Microbiol 7.

[19]. Bhattacharya M, Berends ETM, Chan R, Schwab E, Roy S, Sen CK, Torres VJ, Wozniak DJ. 2018. *Staphylococcus aureus* biofilms release leukocidins to elicit extracellular trap formation and evade neutrophil-mediated killing. Proc Natl Acad Sci 201721949.

[20]. Sultan AR, Swierstra JW, Toom NAL, Snijders SV, Maňásková SH, Verbon A, Wamel WJB van. 2018. Production of Staphylococcal Complement Inhibitor (SCIN) and Other Immune Modulators during the Early Stages of *Staphylococcus aureus* Biofilm Formation in a Mammalian Cell Culture Medium. Infect Immun IAI. 00352–18.

[21]. Guggenberger C, Wolz C, Morrissey JA, Heesemann J. 2012. Two Distinct Coagulase-Dependent Barriers Protect *Staphylococcus aureus* from Neutrophils in a Three Dimensional *in vitro* Infection Model. PLOS Pathog 8:e1002434. [PubMed: 22253592]

[22]. Günther F, Wabnitz GH, Stroh P, Prior B, Obst U, Samstag Y, Wagner C, Hänsch GM. 2009. Host defence against *Staphylococcus aureus* biofilms infection: Phagocytosis of biofilms by polymorphonuclear neutrophils (PMN). Mol Immunol 46:1805–1813. [PubMed: 19261332]

[23]. Thurlow LR, Hanke ML, Fritz T, Angle A, Aldrich A, Williams SH, Engebretsen IL, Bayles KW, Horswill AR, Kielian T. 2011. *Staphylococcus aureus* Biofilms Prevent Macrophage Phagocytosis and Attenuate Inflammation *In Vivo*. J Immunol 186:6585–6596. [PubMed: 21525381]

[24]. Ghimire N, Pettygrove BA, Pallister KB, Stangeland J, Stanhope S, Klapper I, Voyich JM, Stewart PS. 2019. Direct Microscopic Observation of Human Neutrophil-*Staphylococcus aureus* Interaction *In Vitro* Suggests a Potential Mechanism for Initiation of Biofilm Infection on an Implanted Medical Device. Infect Immun 87.

[25]. Alhede M, Lorenz M, Fritz BG, Jensen PØ, Ring HC, Bay L, Bjarnsholt T. 2020. Bacterial aggregate size determines phagocytosis efficiency of polymorphonuclear leukocytes. Med Microbiol Immunol 209:669–680. [PubMed: 32880037]

[26]. Harding MG, Zhang K, Conly J, Kubes P. 2014. Neutrophil Crawling in Capillaries; A Novel Immune Response to *Staphylococcus aureus*. PLOS Pathog 10:e1004379. [PubMed: 25299673]

[27]. McDonald B, Pittman K, Menezes GB, Hirota SA, Slaba I, Waterhouse CCM, Beck PL, Muruve DA, Kubes P. 2010. Intravascular Danger Signals Guide Neutrophils to Sites of Sterile Inflammation. Science 330:362–366. [PubMed: 20947763]

[28]. Bjarnsholt T, van Gennip M, Jakobsen TH, Christensen LD, Jensen PØ, Givskov M. 2010. *In vitro* screens for quorum sensing inhibitors and *in vivo* confirmation of their effect. 2. Nat Protoc 5:282–293. [PubMed: 20134428]

[29]. van Gennip M, Christensen LD, Alhede M, Qvortrup K, Jensen PØ, Høiby N, Givskov M, Bjarnsholt T. 2012. Interactions between Polymorphonuclear Leukocytes and *Pseudomonas aeruginosa* Biofilms on Silicone Implants *In Vivo*. Infect Immun 80:2601–2607. [PubMed: 22585963]

[30]. Yipp BG, Petri B, Salina D, Jenne CN, Scott BNV, Zbytnuik LD, Pittman K, Asaduzzaman M, Wu K, Meijndert HC, Malawista SE, de Boisfleury Chevance A, Zhang K, Conly J, Kubes P. 2012. Infection-induced NETosis is a dynamic process involving neutrophil multitasking in vivo. 9. Nat Med 18:1386–1393. [PubMed: 22922410]

[31]. Hasenberg A, Hasenberg M, Männ L, Neumann F, Borkenstein L, Stecher M, Kraus A, Engel DR, Klingberg A, Seddigh P, Abdullah Z, Klebow S, Engelmann S, Reinhold A, Brandau S, Seeling M, Waisman A, Schraven B, Göthert JR, Nimmerjahn F, Gunzer M. 2015. Catchup: a mouse model for imaging-based tracking and modulation of neutrophil granulocytes. Nat Methods 12:445–452. [PubMed: 25775045]

[32]. Jensen PØ, Bjarnsholt T, Phipps R, Rasmussen TB, Calum H, Christoffersen L, Moser C, Williams P, Pressler T, Givskov M, Høiby N. 2007. Rapid necrotic killing of polymorphonuclear

leukocytes is caused by quorum-sensing-controlled production of rhamnolipid by *Pseudomonas aeruginosa*. Microbiology, 153:1329–1338. [PubMed: 17464047]

[33]. Bjarnsholt T, Alhede M, Alhede M, Eickhardt-Sørensen SR, Moser C, Kühl M, Jensen PØ, Høiby N. 2013. The *in vivo* biofilm. Trends Microbiol 21:466–474. [PubMed: 23827084]

[34]. Lämmermann T, Afonso PV, Angermann BR, Wang JM, Kastenmüller W, Parent CA, Germain RN. 2013. Neutrophil swarms require LTB4 and integrins at sites of cell death *in vivo*. 7454. Nature 498:371–375. [PubMed: 23708969]

[35]. Bogoslowski A, Butcher EC, Kubes P. 2018. Neutrophils recruited through high endothelial venules of the lymph nodes via PNAd intercept disseminating *Staphylococcus aureus*. Proc Natl Acad Sci 115:2449–2454. [PubMed: 29378967]

[36]. Pabst B, Pitts B, Lauchnor E, Stewart PS. 2016. Gel-Entrapped *Staphylococcus aureus* Bacteria as Models of Biofilm Infection Exhibit Growth in Dense Aggregates, Oxygen Limitation, Antibiotic Tolerance, and Heterogeneous Gene Expression. Antimicrob Agents Chemother 60:6294–6301. [PubMed: 27503656]

[37]. Surewaard BGJ, Haas CJC de, Vervoort F, Rigby KM, DeLeo FR, Otto M, Strijp JAG van, Nijland R. 2013. Staphylococcal alpha-phenol soluble modulins contribute to neutrophil lysis after phagocytosis. Cell Microbiol 15:1427–1437. [PubMed: 23470014]

[38]. Voyich JM, Braughton KR, Sturdevant DE, Whitney AR, Saïd-Salim B, Porcella SF, Long RD, Dorward DW, Gardner DJ, Kreiswirth BN, Musser JM, DeLeo FR. 2005. Insights into Mechanisms Used by *Staphylococcus aureus* to Avoid Destruction by Human Neutrophils. J Immunol 175:3907–3919. [PubMed: 16148137]

[39]. Voyich JM, Vuong C, DeWald M, Nygaard TK, Kocianova S, Griffith S, Jones J, Iverson C, Sturdevant DE, Braughton KR, Whitney AR, Otto M, DeLeo FR. 2009. The SaeR/S Gene Regulatory System Is Essential for Innate Immune Evasion by *Staphylococcus aureus*. J Infect Dis 199:1698–1706. [PubMed: 19374556]

[40]. Christensen LD, Moser C, Jensen PØ, Rasmussen TB, Christophersen L, Kjelleberg S, Kumar N, Høiby N, Givskov M, Bjarnsholt T. 2007. Impact of *Pseudomonas aeruginosa* quorum sensing on biofilm persistence in an *in vivo* intraperitoneal foreign-body infection model. Microbiology 153:2312–2320. [PubMed: 17600075]

[41]. Cavanagh JP, Granslo HN, Fredheim EA, Christophersen L, Jensen PØ, Thomsen K, Van Gennip M, Klingenberg C, Flaegstad T, Moser C. 2013. Efficacy of a synthetic antimicrobial peptidomimetic versus vancomycin in a *Staphylococcus epidermidis* device-related murine peritonitis model. J Antimicrob Chemother 68:2106–2110. [PubMed: 23645587]

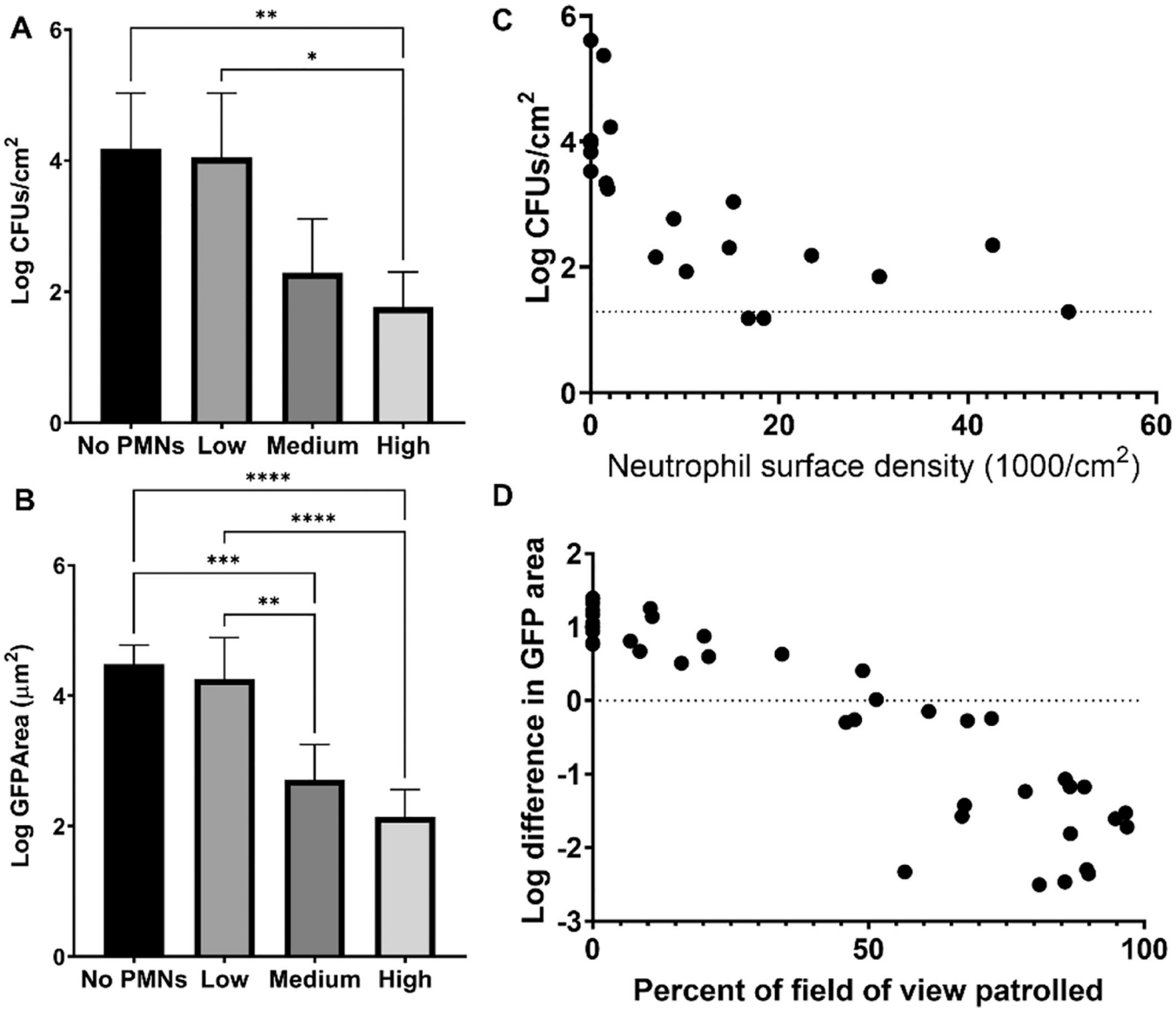

Figure 1:

High neutrophil densities are required for adequate clearance of attached *S. aureus in vitro*. Approximately 2×10^3 CFUs/cm^2 *S. aureus* GFP were initially added to the surface and challenged with PMNs for 4 h. (A) *S. aureus* CFUs recovered and (B) total remaining GFP signal from wells with no, low ($1.7 \pm 0.27 \times 10^3$ PMNs/cm^2), medium ($1.0 \pm 0.31 \times 10^4$ PMNs/cm^2), or high ($2.8 \pm 1.3 \times 10^4$ PMNs/cm^2) numbers of PMNs. Data are mean ± SD (n=4–7. Kruskal-Wallis Test (panel A) and one-way ANOVA with Tukey's post hoc test (panel B) **p<0.01, ***p<.001, **** p<0.0001). (C) CFUs recovered from challenge plotted against varied neutrophil surface densities. Dashed line represents limit of detection. n=5 independent experiments. (D) Log difference in GFP area per field of view as a function of the percentage of the field of view covered by neutrophil tracks. n=40 FOVs from 5 independent experiments.

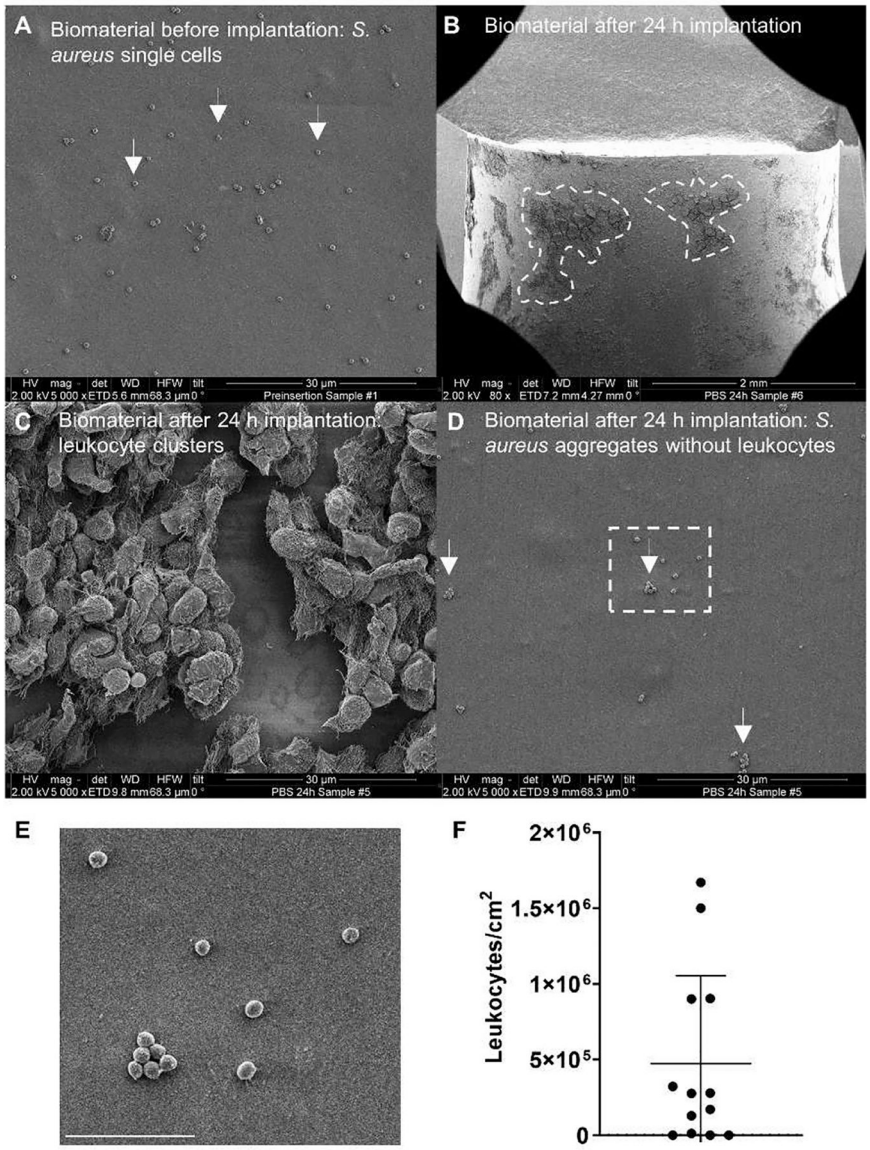

Figure 2:

Immune cell recruitment to an inoculated peritoneal implant is heterogeneous. (A) SEM micrographs showing adherent *S. aureus* cells on the surface of a silicone tube prior to implantation into the mouse peritoneum. (B-D) Representative SEM micrographs from silicone tubes removed from the mouse peritoneal cavity after 24 h. (B) At low (80x) magnification, distinct areas of significant immune cell recruitment can be observed as dark patches on the implant surface (highlighted by dashed lines). (C) Higher magnification (5000x) reveals the dark patches outlined in (B) to be leukocyte clusters. (D) Higher magnification (5000x) reveals sections of the implant devoid of leukocytes. (E) Inset of the region denoted by the white box in (D). Scale bar = 5 μm. (F) Estimated leukocyte numbers on the implant surface from SEM images, normalized to FOV area (n=13 FOVs).

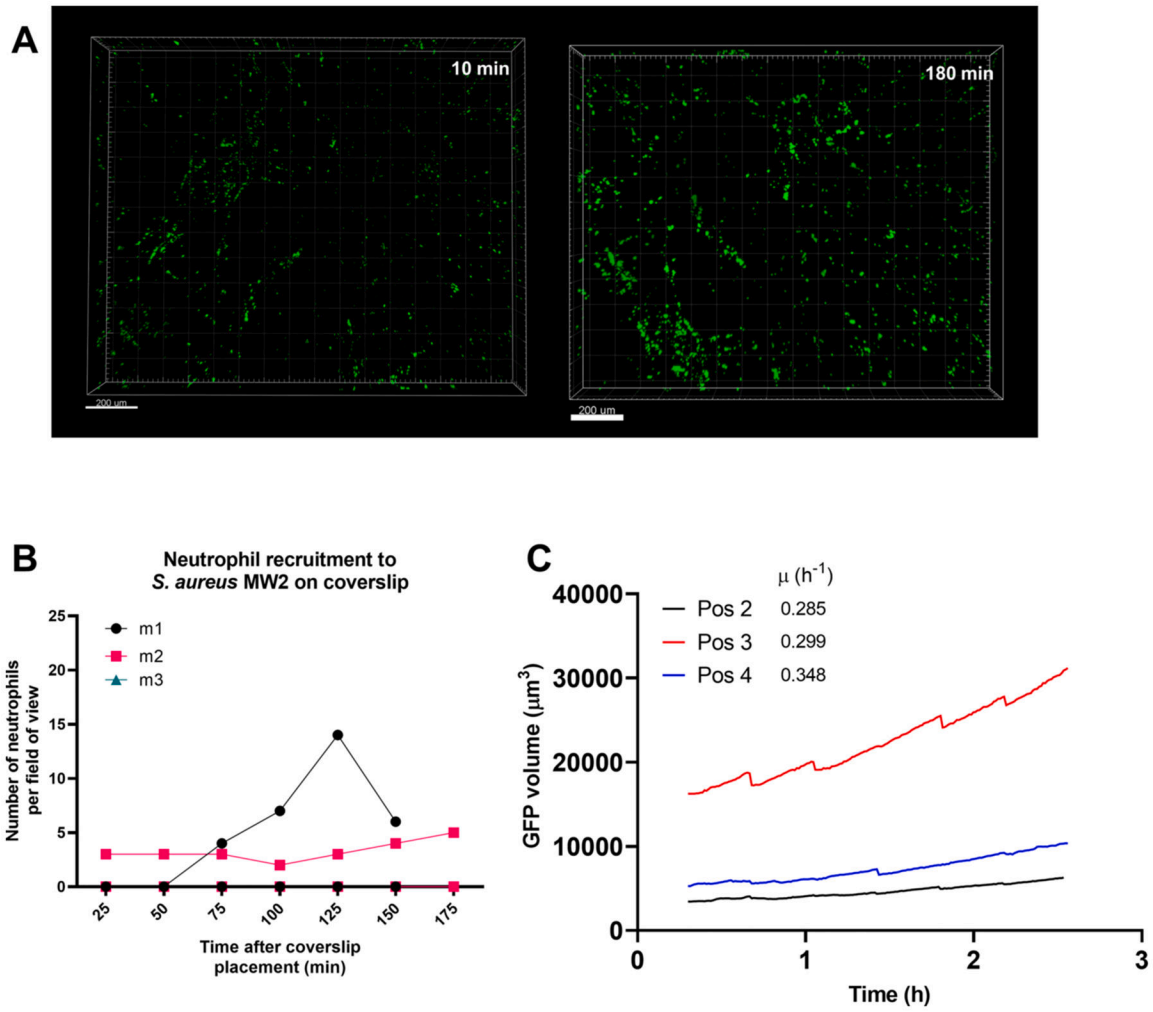

Figure 3:

S. aureus aggregates become resilient to neutrophil clearance after four hours of growth *in vitro*. *S. aureus* (green) clusters were seeded at ~10^2 CFUs/cm^2 and grown for 4 h (HS) or seeded at ~10^3 CFUs/cm^2 and grown for 0.5 h (No HS) prior to the start of imaging, with or without neutrophil (red) addition (~2×10^4 PMNs/cm^2). (A) Representative microscopy images at t = 0 h and t = 4 h. (B) Log CFUs/cm^2 recovered from wells post imaging. (C) Log difference in CFUs/cm^2 (black points) and GFP area (white points). Data are mean ± SD (n=4 independent experiments. Paired student's t-test *p<0.05, **p<0.01.).

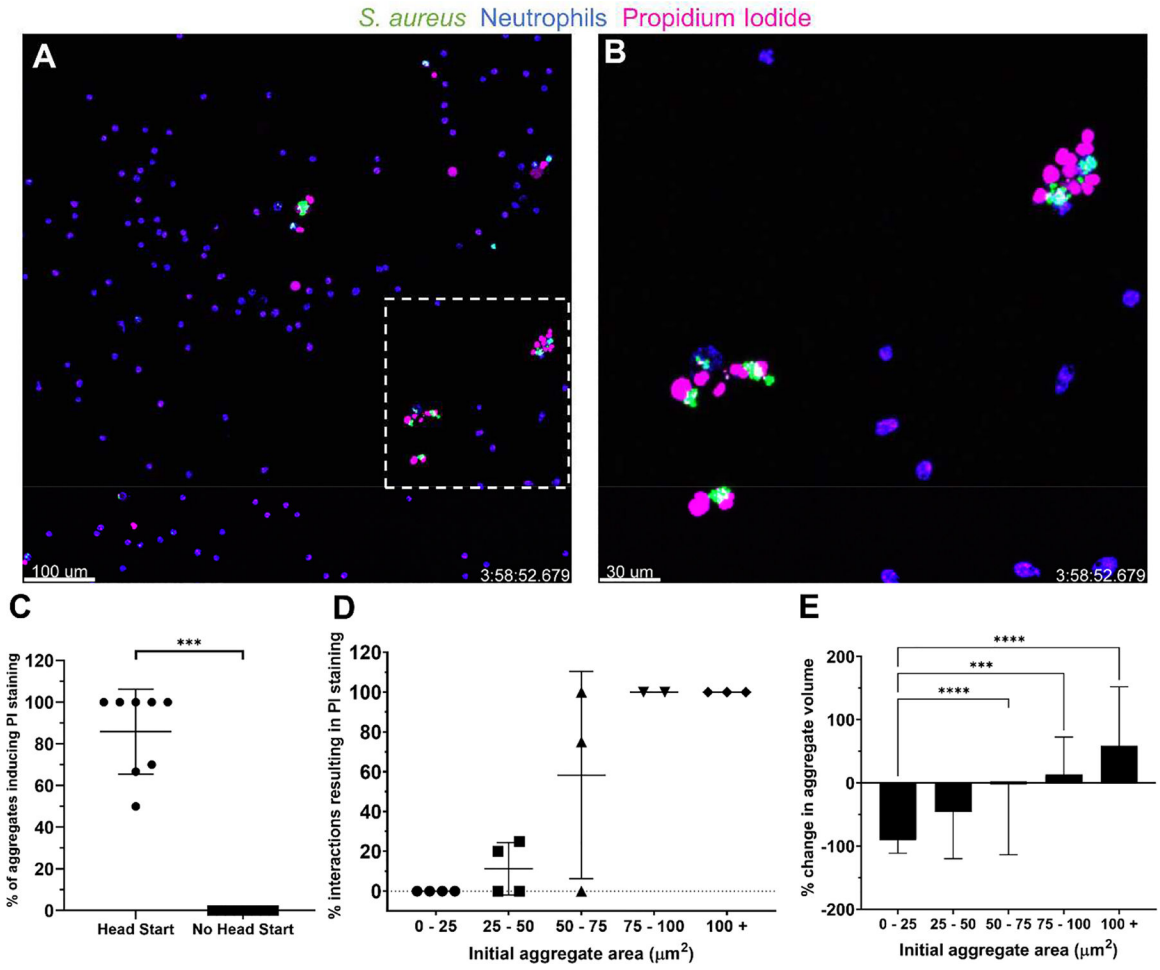

Figure 4:

Larger *S. aureus* aggregates cause neutrophil lysis and resist clearance *in vitro*. (A) *S. aureus* aggregates (green) were given 4 h to grow prior to the addition of neutrophils (blue). Representative images at t = 4 h show propidium iodide (PI) staining (pink) of neutrophils interacting with larger, persistent clusters of *S. aureus*. (B) Enlarged image of the inset in (A). (C) Percentage of *S. aureus* aggregates causing PI staining of at least one neutrophil. Data are mean ± SD (n=8 FOVs per group from 4 independent experiments. Mann-Whitney test ***p<.001). (D) Rates of PI staining of neutrophils as a function of the bacterial aggregate area at the beginning of the interaction. Each point represents the calculated average of all interactions within the size boundaries from a given experiment. The number of observed interactions per point ranged from n = 1–19 collected from 16 FOVs from 4 independent experiments. (E) Change in volume of an aggregate from the first frame in which a neutrophil phagocytoses it to the last frame that it is visible. Data are mean ± SD (Bins contain 6–58 measurements from 16 FOV from 4 independent experiments. Kruskal-Wallis test ***p<0.001, ****p<0.0001).

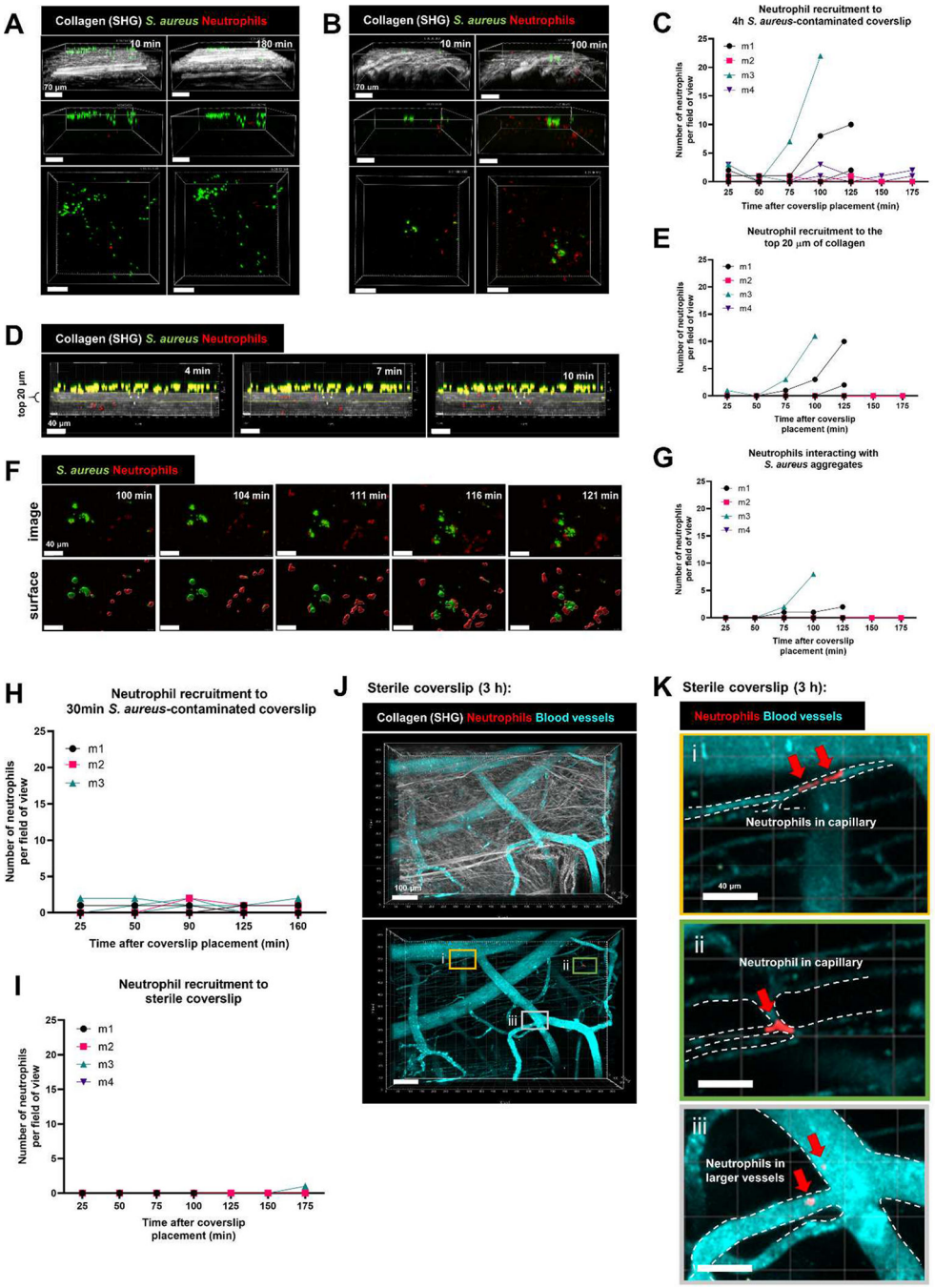

Figure 5:

Minimal neutrophil recruitment to a *S. aureus*-contaminated coverslip *in vivo*. *S. aureus* aggregates were given 4 h to grow prior to placing the coverslip onto the dermal skin flap for intravital imaging. Representative 3D images of (A) minimal neutrophil recruitment and (B) moderate neutrophil recruitment at 10 min and 180 min after coverslip placement onto skin flap. Top: side view showing collagen (SHG) signal, middle: side view without collagen, bottom: top view without collagen. Scale bars = 70 μm. (C) Quantification of neutrophil recruitment to the 4 h *S. aureus*-contaminated coverslip. (D) Representative timelapse

images of neutrophils (red spots) trafficking through the collagen into the top 20 μm. Scale bars = 40 μm. (E) Quantification of the number of neutrophils in the top 20 μm of collagen. (F) Representative timelapse images of neutrophils interacting with *S. aureus* aggregates at the coverslip surface over the course of 20 min. Scale bars = 40 μm. (G) Quantification of the number of neutrophils interacting with *S. aureus*. Quantification of (H) neutrophil recruitment to a single-cell 30-minute attached *S. aureus*-contaminated coverslip and (I) sterile coverslip. (J) Representative 3D stitched image of a sterile coverslip after 180 min of imaging, showing dermal collagen (white), blood vessels (cyan) and neutrophils (red). Bottom: identical 3D image without collagen. Scale bars = 100 μm. Three boxes (i, ii, iii) are selected to show one or two neutrophils in capillaries (K i, ii) and two neutrophils in larger dermal blood vessels (K iii). Scale bars = 40 μm. For C,E,G,H,I, n=3–4 mice from 3–4 independent experiments listed as m1, m2, m3, m4. Data show 3 fields of view per mouse.

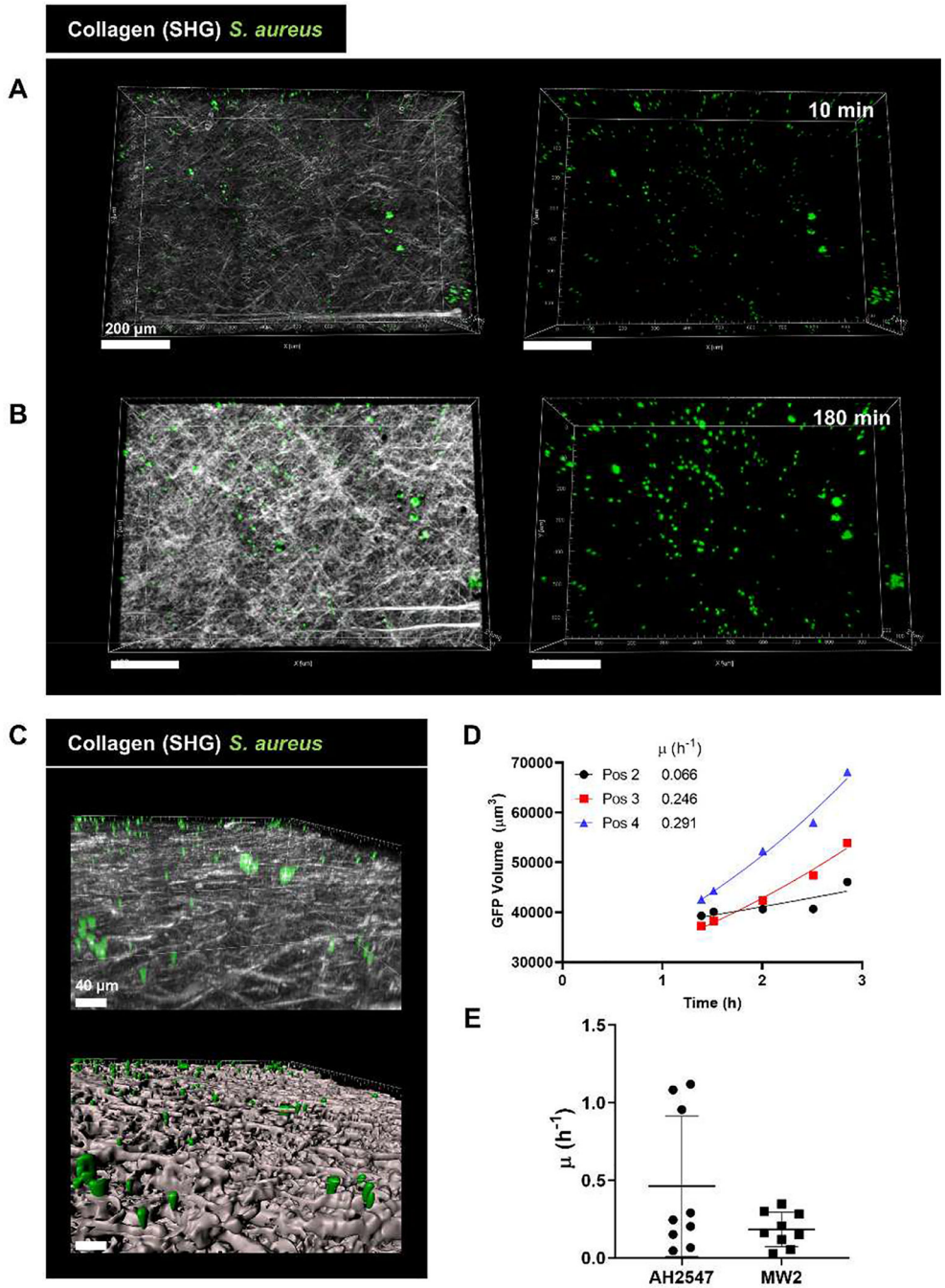

Figure 6:

S. aureus aggregates grow on the coverslip *in vivo*. (A) Representative intravital image of a 3D region recorded at (A) start of imaging (10 min after coverslip addition) and (B) end of imaging (180 min after coverslip addition). Left: collagen (white) and *S. aureus* (green), right: *S. aureus* signal only. Scale bars = 200 µm. (C) 3D reconstruction of the coverslip surface coverslip showing GFP *S. aureus* in close contact with collagen. Top: 3D image, bottom: surface reconstruction with Imaris. Scale bars = 40 µm (D) Representative quantification of *S. aureus* growth *in vivo* over 180 min of imaging with an exponential

curve fit to the data. Reported value μ represents the specific growth rate satisfying the equation $X = X_0 e^{\mu t}$. Data shown includes representative points outside of lag phase from one mouse with three fields of view. (E) Growth rate values measured *in vivo*. Points represent value measured from a single FOV. Error bars indicate mean ± SD. (n=3 mice/condition with 3 FOV per mouse).

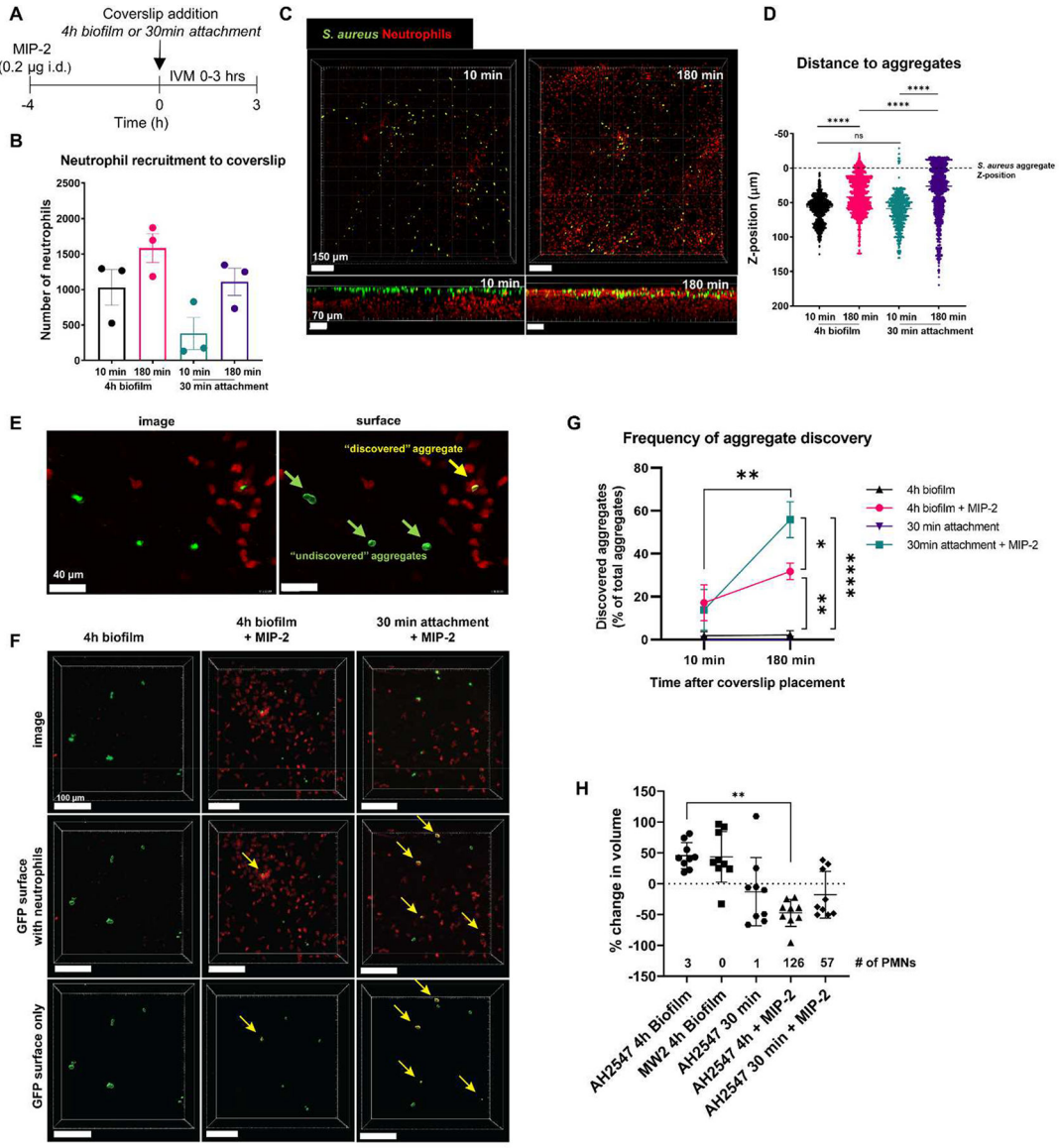

Figure 7:

Pre-recruitment of neutrophils to the skin results in *S. aureus* aggregate discovery and increased clearance. (A) Experimental timeline for MIP-2 treatment and intravital microscopy. (B) Quantification of neutrophil recruitment at 10 min and 180 min after coverslip placement. Error bars indicate the mean ± SEM (n=3/condition, one-way ANOVA with Tukey's post-hoc test). (C) Representative 3D stitched image showing neutrophil migration through the z-plane towards *S. aureus* on the coverslip at 10 min and 180 min after coverslip placement. Top panels show XY plane viewed from the top (scale bars = 150 μm), bottom panels show XZ plane viewed from the side (scale bars = 70 μm). (D) Quantification of neutrophil distance to *S. aureus* aggregates. Z-position was normalized to the averaged Z-position of *S. aureus* aggregates at each time point. Dashed line indicates the average z-position of *S. aureus* aggregates. Each dot represents one neutrophil. Data are mean ± SEM (n=3 mice/condition, one-way ANOVA $p<0.0001$, Tukey's post hoc test **** $p<0.0001$). (E)

Representative image showing one bacterial aggregate discovered by neutrophils and three other bacterial aggregates that remain undiscovered. Left: intravital image, right: surface reconstruction with a filter applied to label the discovered bacteria aggregate (yellow) and undiscovered aggregates (green). Scale bars = 40 μm. (F) Representative intravital images of aggregate discovery. Left: 4 h biofilm with no MIP-2 treatment. Middle: 4 h biofilm with MIP-2 treatment. Right: 30 min attachment with MIP-2 treatment. Yellow arrows point to discovered aggregates. Scale bars = 100 μm. (G) Quantification of aggregate discovery across the three conditions: 4 h biofilm, 4 h biofilm + MIP-2, 30 min attachment + MIP-2. Data show discovered aggregates as a percent of total aggregates at select time points 10 min and 180 min after coverslip placement. Data are mean ± SEM (n=3 mice/condition, Two-way RM ANOVA $p<0.01$, Tukey's post hoc test *$p<0.05$, **$p<0.01$, **** $p<0.0001$ compared between groups at the indicated time point, Bonferroni's multiple comparisons test **$p<0.01$ compared over time within the same group). (H) Percent change in GFP volume between the last frame and first frame for the final continuous FOV for each position. Numbers above the x-axis indicate the average number of neutrophils in the FOV at the end of imaging. Data mean ± SD (Each data point indicates one FOV, n=3 mice/condition, Kruskal-Wallis Test *$p<0.05$, ***$p<0.001$).